Francis-99: Coupled simulation of the resonance effects in runner channels

IOP Conf. Series: Journal of Physics: Conf. Series **1296** (2019) 012005 doi:10.1088/1742-6596/1296/1/012005

Francis-99: Coupled simulation of the resonance effects in runner channels

Erik Tengs[1,2], **Live Salvesen Fevåg**[1], **Pål-Tore Storli**[2]

[1] EDR&Medeso, Leif Tronstad Plass 3, 1337 Sandvika, Norway
[2] Norwegian University of Science and Technology, 7491 Trondheim, Norway

E-mail: erik.tengs@edrmedeso.com

Abstract. A resonance phenomenon is observed experimentally in the runner channels of the Francis-99 model turbine runner. An incompressible CFD simulation is unable to simulate this. Two different coupled physics schemes are therefore presented to investigate if such effects can be replicated through simulations. The first procedure is a fully coupled acoustic-structural simulation, where the surrounding fluid is modelled using acoustic theory. This includes added mass effects and pressure propagation, but not advective and viscous effects. The second procedure is a quasi two-way coupled Fluid-Structure approach based on modal decomposition of the structural domain. In this procedure, the incompressible Navier-Stokes equations are solved along with the structural deformation.

The fully coupled acoustic-structural approach does successfully exhibit a magnification of the pressure through the runner channels, indicating a resonance effect. The exact values of the acoustic pressure amplitudes are highly sensitive to the damping, the blade connection to the shroud close to the trailing edge, and more.

The second procedure manages to simulate the structural deformation with the correct nodal diameters excited by the Rotor Stator Interaction, all inside the fluid solver. The pressure amplitudes however, does not exhibit the desired resonance effect, likely due to the assumption of incompressible fluid.

1. Introduction

Fluid-Structure Interaction (FSI) is a phenomenon that occurs in many physical fields. In general, all phenomena where there is a mutual interaction between a fluid and a structure can be classified as FSI problems, but it usually catches the public interest when catastrophic failures happen. The most famous incident is the Tacoma bridge collapse [1], but it is also seen in many fatal turbine failures in the hydro power industry [2]. The rise of the use of numerical tools have given engineers a better chance of discovering such design flaws early in the process. The tools are not perfect however, and continuous testing, development and validation with experiments are needed to ensure optimal results.

The Francis-99 workshops is a series of three workshops that aims to provide a meeting place for numerical engineers, and provide experimental data for validation of different numerical tools [3]. The open-geometry Francis-99 turbine at the Waterpower Laboratory at NTNU is the basis for discussion, and the different workshops focus on different topics, see i.e. a review of the first workshop regarding CFD [4]. The third workshop discusses FSI, with two test cases made available for the public.

One of the test cases available for the third workshop of the Francis99 research project deals resonance in runner channels. Figure 1 and 2 is taken from [3, 5] and shows the following;

The Francis-99 model runner have been operated in the laboratory at different rotational speeds. As the number of guide vanes and runner blades are constant, this will result in different excitation frequencies in the runner, created by Rotor Stator Interaction (RSI). The turbine has four pressure probes PTR1-4, sequentially placed along the channel, see [5] for more. Figure 1 shows $P_E = p'/gH$, the pressure fluctuation normalized as a percentage of the specific energy in the machine, of the first pressure harmonic. Firstly, we observe that there seems to be a close to constant pressure amplitude for the different rotational speeds, and secondly, the pressure decreases through the channel. This is how we would expect a viscous fluid system to behave. Viscous dissipation dampens the pressure amplitudes through the channel [6]. However, if we turn our attention to figure 2, which shows the amplitude of the *second* pressure harmonic, we see something completely different. Firstly, there is a peak in the pressures around $f \approx 280Hz$, and secondly, at the peak, the pressure is no longer decreasing through the channel. At $f \approx 280Hz$, it is seen that PTR2 and PTR3 have higher pressure amplitudes than PTR1 and PTR4. This may indicate a coupled physics system. The structure is excited by the pressure forces at a frequency close to its natural frequency, and a magnification of the pressure occurs.

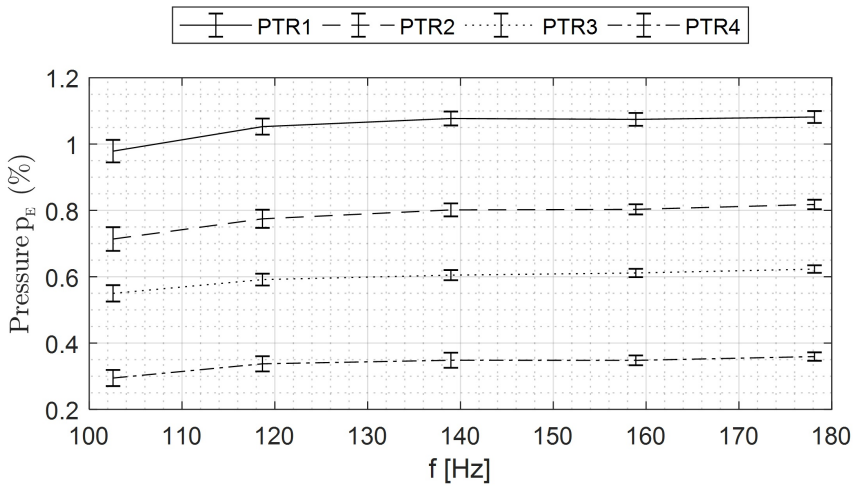

Figure 1. Pressure amplitudes at RSI frequency [3]

In general, for transient, incompressible CFD analysis, the trend showed in figure 1 , i.e. a dampening of the pressure amplitudes through the runner, is observed for both the first and the second pressure harmonic. This is shown earlier in the Francis-99 workshops, and also in the HiFrancis research project [7, 8]. Interestingly, the cited references predict the first harmonic of the pressure field very well, but underestimates the second harmonic. This is another indication that there is no resonance at the first pressure harmonic, but there is one at the second. This illustrates the shortcomings of only performing a CFD analysis, and in this article we wish to expand on this and simulate coupled physics, namely include the structural deformation in the simulations. In short, this article wishes to simulate the effect shown in figure 2 by the use of coupled fluid-structure simulations.

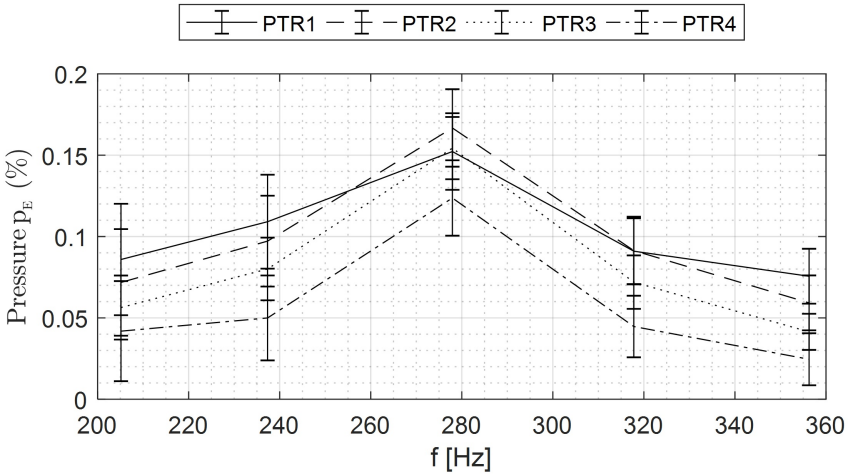

Figure 2. Pressure amplitudes at 2·dRSI frequency [3]

2. Theory and methods

Let us define some key terms regarding Fluid-Structure Interaction (FSI). A step-wise coupled simulation denotes a simulation where information passes from one of the physical domains to the other. The information can go one way, known as a one-way coupled simulation, or it can go both ways, a two-way coupled simulation. An example of a one-way coupled simulation is to perform a steady CFD analysis of a turbine runner, and map the pressure field onto a static structural analysis. If the structural deformation is sent back to the CFD solver to update the fluid domain, it becomes a two-way coupled simulation. See [9] for a thorough comparison between one- and two-way coupled simulations.

A third variant, a *fully coupled*/ monolithic simulation denotes a simulation where the two physical domains are solved for simultaneously, using a single system of equations, common mesh and discretization schemes. This is rarely done in commercial software for viscous flow, however is common practice for structural analysis when the surrounding fluid asserts an added mass effect. It is therefore important to keep in mind that a two-way coupled simulation is *not* a fully coupled simulation. The principle is completely different, as is the usage and availability.

This article will present both a fully coupled simulation and a two-way coupled simulation on the Francis-99 turbine. The following sections will go into more detail on the different approaches, starting with the acoustic-structural simulations.

2.1. Acoustic-Structural simulations

When submerged in water, the dynamic properties and response of a structure is altered by the surrounding heavy fluid. To account for the added mass effects of the fluid, a coupled acoustic-structural simulation can be performed. In ANSYS, this is done by modelling the surrounding fluid using the wave equation [10]. The fluid is primarily defined by its density and speed of sound, such that added mass from the forces on shared surfaces, and pressure propagation in the fluid domain, is considered.

The wave equation can be written on a form similar to the second order structural equation and combined to a *coupled* set of equations. The equation solved for in coupled acoustic-structural equations is referred to as the Eulerian displacement-pressure formulation [10, 11, 12]:

$$\left(-\omega^2 \begin{bmatrix} M_s & 0 \\ M_{fs} & M_a \end{bmatrix} + i\omega \begin{bmatrix} C_s & 0 \\ 0 & C_a \end{bmatrix} + \begin{bmatrix} K_s & K_{fs} \\ 0 & K_a \end{bmatrix}\right) \begin{Bmatrix} u \\ p \end{Bmatrix} = \begin{Bmatrix} F_s \\ F_a \end{Bmatrix} \tag{1}$$

Where M, C, K, F are the mass, damping, stiffness and force matrix respectively. u is the structural displacement, p is the acoustic pressure, and ω is the natural frequency. The subscripts s, a, fs denote structure, acoustic, and fluid-structure respectively. The cross-multiplication matrices (M_{fs}, K_{fs}) are obtained by enforcing boundary conditions on the fluid-structure interface. This ensures that information will cross the domain interfaces in a consistent way. The derivation of eq. 1 can be found in Appendix A.

Nodal Diameters. We want to find evidence of resonance in the runner by performing a coupled acoustic-structural simulation. First a modal analysis can be performed. Given that the dominant load frequencies, f_{RSI}, in the system are known,

$$f_{RSI} = n \cdot f_{runner} \cdot Z_{gv}, \quad n = 1, 2, ..., \tag{2}$$

a modal analysis will reveal if there are any eigenfrequencies in this range. Z_{gv} denotes the number of guide vanes. Matching loading frequency and eigenfrequency is a *necessary* but not *sufficient* condition to cause resonance. Additionally, the spatial distribution of the load has to match the spatial distribution of the eigenmode. This is illustrated in figure 3, where a eigenmode of a string is shown along with two forces. Even if the frequency of load F_2 is equal to the eigenfrequency of the string, the mode will not be exited as the load is placed at a node. Force F_1 however, will excite the given eigenmode, and resonance will occur if the load- and eigenfrequency matches.

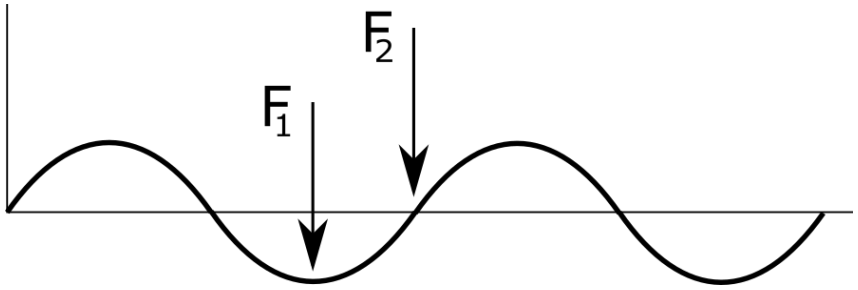

Figure 3. Conceptual resonance conditions

For a disc-like structure like a turbine, this generalizes to the concept of Nodal Diameters (ND). The ND of the symmetric, rotating pressure pattern created by RSI is determined by the number of stationary and rotating components [13, 14];

$$ND = mZ_r \pm nZ_{gv}, \quad m, n = 1, 2, ..., \tag{3}$$

Where m,n are integers, and Z_r, Z_{gv} is the number of runner and guide vanes respectively. Resonance can occur if the loading frequency matches a runner eigenfrequency with a corresponding mode characterized by the same nodal diameter.

For the Francis-99 runner, we have at design; $Z_r = 30, Z_{gv} = 28, f_{runner} = 333[rpm]$. By using this in eq. 2 and 3, we can sum up the expected critical behavior as follows; The turbine can be excited at ND2 at $f_{RSI1} = 155Hz$, at ND4 at $f_{RSI2} = 310Hz$, for $n = m = [1, 2]$. Higher harmonics are also possible, although the lowest modes are most likely to be excited. As discussed earlier, in the laboratory, the runner was operated in a range of rotational speeds to increase the chance of finding resonance conditions.

A preliminary modal analysis was performed on the Francis-99 turbine. No ND2 modes were found with eigenfrequencies in the range $f = [100 - 180][Hz]$, however an ND4 mode

was found with in the range $f = [200 - 360][Hz]$. This corresponds well with figures 1 and 2. However, as stated in the problem text, the goal of the present work is not to find the exact eigenfrequency, but to find the resonance phenomenon. This means that the applied load in the coming simulations will correspond to the eigenfrequency found in the simulations, rather than matching the one seen in figure 2. The following section will outline the procedure of performing a harmonic analysis of the turbine excited by an ND4 pressure field.

2.1.1. Numerical Procedure. The simulations are performed using ANSYS Mechanical Enterprise Release 19.2. The numerical model is created as perfectly symmetric assembly of 15 sectors. Figure 4 shows the structural parts, with material assignment of copper alloys JM7 and JM3 [15] to the hub/shroud and blades respectively. Instrumentation, holes and more present in the Francis-99 model turbine are omitted. Bolts and bolt holes are not modelled, instead the blades are attached to the hub and shroud by bonded contact, defined on the surfaces that will be press-fit by the bolts, as seen in red in Figure 5. As discussed in the workshop test case description [3], there is some uncertainty with regards to the fixation of the blades to the shroud towards the trailing edge. The edge in question, marked with blue in Figure 5, is kept free to move relative to the shroud. The acoustic domain is shown in Figure 6. Water with default ANSYS values for density and speed of sound is used as fluid.

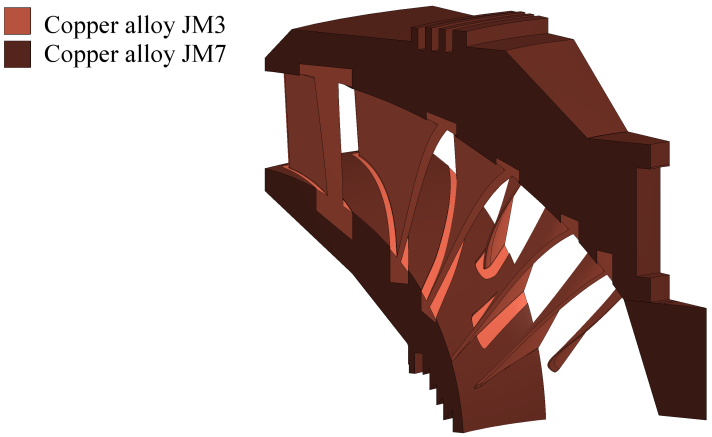

Figure 4. Runner geometry with material assignment. One of 15 identical sectors displayed

For the runner, the element size is limited to 14 mm, with refinement of 4.5 mm assigned to the blades. The total number of nodes is $2 \cdot 10^6$. Table 1 lists the estimated discretization error for selected outputs using the Grid Convergence Index (GCI) [16]. f_n denotes the eigenfrequency, and PT1-4 denotes the pressure amplitudes in the four probes of figure 1. All errors are well below 1%, and the mesh is assumed to produce a converged solution.

The analyses are run as full harmonic analyses using the distributed sparse direct solver. The runner is fixed in space at the hub, replacing the connection to the shaft. Reflective boundaries are specified at all acoustic boundaries. Interaction occurs at the interface between the structural and acoustic domain through shared nodes.

Damping is represented as beta damping, from the concept of proportional or Raleigh damping [17];

$$\beta = \frac{2\xi}{\omega} \tag{4}$$

where β is the frequency dependent, stiffness proportional damping coefficient, and ξ is the

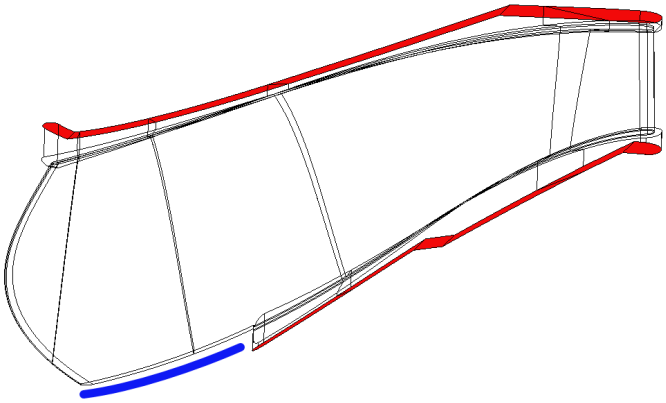

Figure 5. Runner blade. Contact to hub and shroud highlighted

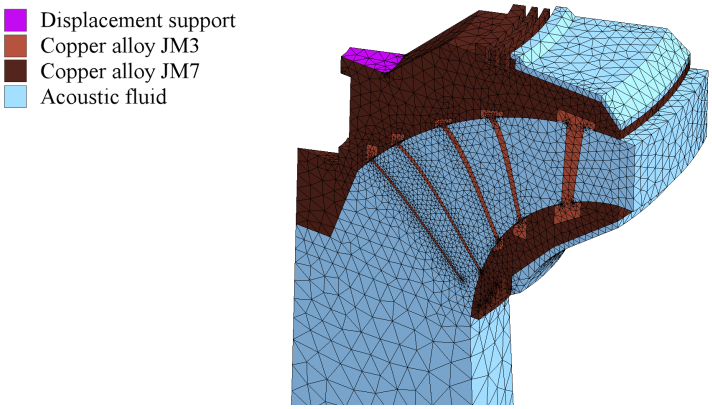

Figure 6. Acoustic and structural elements. One of 15 identical sectors displayed

Table 1. Discretization error

Indicator	GCI error
f_n	0.7 %
PT1	0.0 %
PT2	0.5 %
PT3	0.1 %
PT4	0.1 %

damping ratio. In Agnalt et. al [5], the damping in this experiment was estimated using least squares fitting to be in the range $\xi = [2.5\% - 5.1\%]$.

The load applied in the structural-acoustic simulation is taken from an incompressible CFD simulation, [8]. The load is imported as Fourier coefficients A_i, B_i, with i being 2 for the second pressure harmonic. The Fourier coefficients are applied as a surface load at the runner channel surfaces. This way, the load does not constrain the acoustic pressure degree of freedom in the acoustic domain, instead acts as a load on the structural domain.

The structural response is highly nonlinear with respect to the damping ratio ξ as well as the difference in loading frequency and eigenfrequency, especially close to resonance conditions.

To evaluate the sensitivity of these parameters, simulations are set up with damping values $\xi = [1, 3, 5]\%$ and the load frequency is specified to be within $\pm 7.5\%$ of the eigenfrequency found in the modal analysis. A simulation run at numerical resonance with 3% damping is selected as the reference case.

2.2. Two-way coupled simulation

The traditional way of performing a two-way simulation is to set up both a fluid and a structure simulation separately, and during the execution process pass information from one domain to the other. The usual information flow is as follows; the fluid domain passes on the pressure forces on the fluid-structure interfaces, and the structural domain passes back the structural deformation. The mesh used in the fluid simulation will then deform accordingly and the calculation will continue. Usually this is done in an implicit manner for each time-step, meaning that there is an iterative procedure until a certain convergence criterion is met.

In the procedure chosen in this paper, a quasi two-way approach is used. This procedure applies a modal decomposition to the structural domain, expresses the structural deformation as a set of linearly independent equations, and solves the system inside the iterative fluid solver. This means that there is only need for one solver, in this case ANSYS CFX, a significant speedup. See figure 7 for a simplified flowchart. If the structural domain is discretized using a Crank-Nicolson scheme, the modal deformation and velocity can be described as follows;

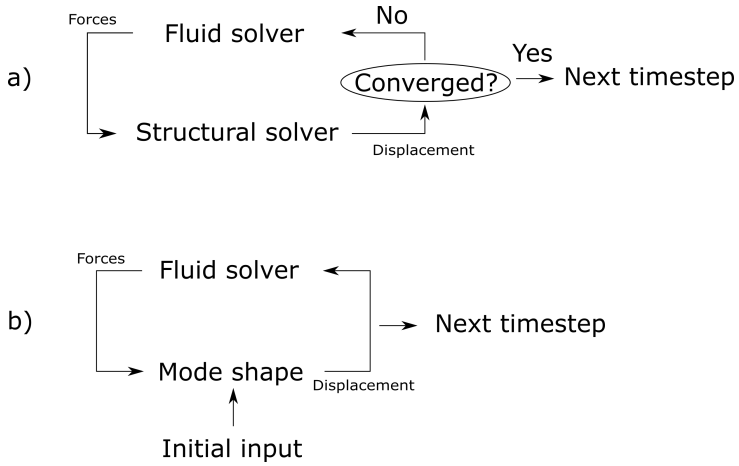

Figure 7. Flow chart describing a) Two-way procedure, b) Quasi two-way procedure

$$q_{i,k+1} = \frac{q_{i,k}(1 + \omega\xi\Delta t - \frac{1}{4}\omega^2\Delta t^2) + \Delta t v_{i,k} + \frac{1}{4}\Delta t^2(f_{i,k+1} + f_{i,k})}{1 + \omega\xi\Delta t + \frac{1}{4}\omega^2\Delta t^2} \tag{5}$$

$$v_{i,k+1} = 2\frac{q_{i,k+1} - q_{i,k}}{\Delta t} - v_{i,k} \tag{6}$$

where $q_{i,k}, v_{i,k}$ denotes the modal amplitude and velocity of mode i at timestep k. The derivation of the above expressions and the theory behind can be found in [18].

2.2.1. Numerical procedure. The runner mesh was created in ANSYS TurboGrid, as one section consisting of one main and one splitter blade. The final mesh consisted of 15 of this section, to eliminate any error linked to unsymmetrical mesh. Figure 8 shows the mesh on the hub, around the main and splitter blades. The same mesh was used in reference [19], and indicates

that the GCI discretization error is $< 0.5\%$ for global parameters. On the inlet of the runner the total pressure profile from a simulation with spiral casing, guide vanes and full draft tube was prescribed, taken from [8].

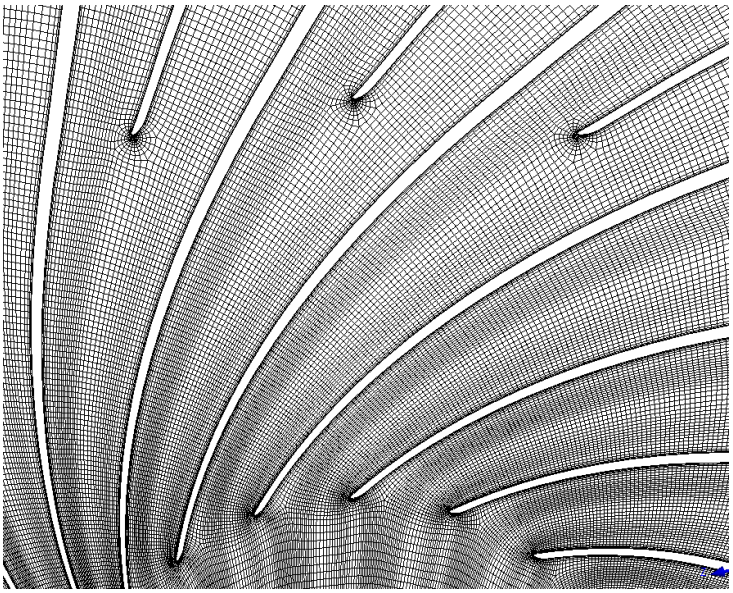

Figure 8. CFD mesh at hub, detailing blade outlet

A modal analysis of the runner will result in a complex mode shape. A complex mode contains a real and complex component, but is easiest understood as a mode where all parts of the structure does not reach its maximum deflection at the same time. A generic representation, $A(x, y)sin(\omega t)$ is therefore insufficient to describe the whole structure, and a second sinusoid is needed. Due to the real nature of equation 5-6, this mode could not be directly imported into the current setup. Instead, a local (real) blade mode was imported to each blade, and set to be free to move independently of each other. Any complex mode shapes would then be created by the pressure field induced by the RSI effects. This is a simplification, but it works for demonstration purposes.

3. Results and Discussion

3.1. Acoustic-Structural simulations

This section will present the results from the acoustic-structural simulations. Figure 9 shows the total simulated pressure compared with the experimental results provided by the workshop committee. The pressure from the numerical simulations is the sum of the convective pressure from an uncoupled CFD analysis [8] and the acoustic pressure from the reference case using 3% damping at resonance.

There is a very good match with the experiments, especially in the beginning of the channel, where the values are close to identical. The shape of the pressure distribution through the channel also corresponds well, although the pressure amplitude at the outlet, PT4, is underestimated. Reasons for this will be discussed. Figure 10 shows the convective and acoustic components of the pressure for both the numerical and experimental results. The experimental results are taken from the workshop website [3], as well as reconstructed from [5].

Figure 9 shows an overall good agreement between the numerical simulations and the experiments. In figure 10 however, we see that virtually all of the error is in the acoustic

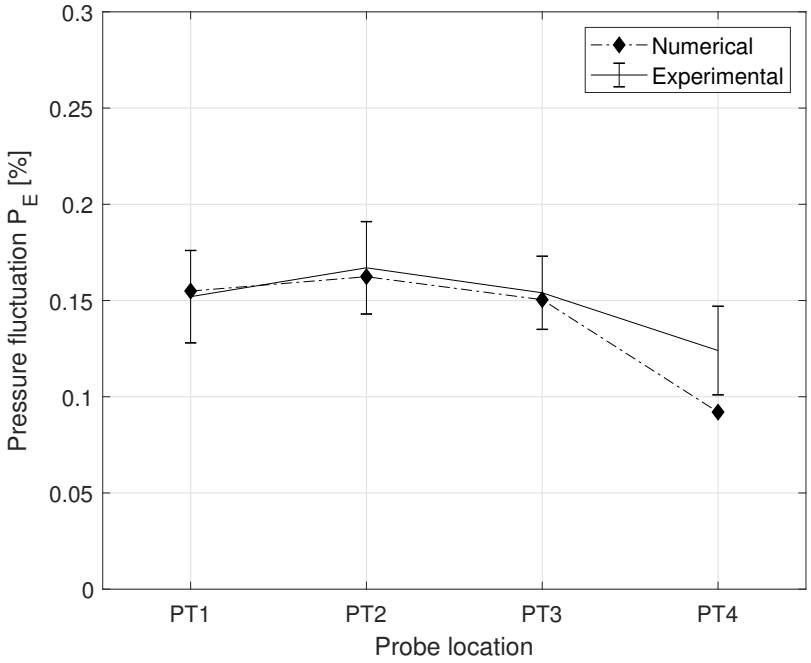

Figure 9. Numerical and experimental pressure amplitudes

part of the pressure, as the convective part is very well predicted. Of several possible reasons, two assumptions have been identified as significant and will be presented below.

Damping. Figure 11 shows the experimental results combined with an uncertainty band indicating the sensitivity to damping. An immediate observation is the strong dependence on the damping, and also the non-linearity of the relation. Increasing the damping from $1\% - 3\%$ significantly reduces the response, while increasing from $3\% - 5\%$ is not as severe. As mentioned, the damping used here is based on Agnalt et. al [5], who estimated the damping to be in the range $\xi = [2.5\% - 5.1\%]$. If such an estimate is unavailable, a flutter analysis should be performed to obtain a reasonable damping estimate. This has been done previously with good results by i.e [20]. The effect of the load not being equal to the eigenfrequency was also tested. Going by figure 2 and its reference [5] it is estimated that the experiment was performed within a couple of percent from the eigenfrequency. In this range, the effect of different damping ratios is dominating, although a combined effect is seen. I.e. with low damping, the response is more sensitive to how close the load is to the resonance peak. Conversely, high damping makes the resonance peak flatter.

Effect of blade fixation. The bolted geometry of the Francis-99 model turbine makes the numerical simulations especially complex. Replacing the bolts by contacts, as performed in this paper, is an assumption. Additionally, there is some uncertainty with regards to the fixation of the blades to the shroud towards the trailing edge.

To investigate the impact of the connection between blades and shroud, a simulation was performed with a bonded contact at the edge marked blue in figure 5, fully fixating the blade to the shroud.

Figure 12 shows the results from simulations with different fixation of the edge in question. As

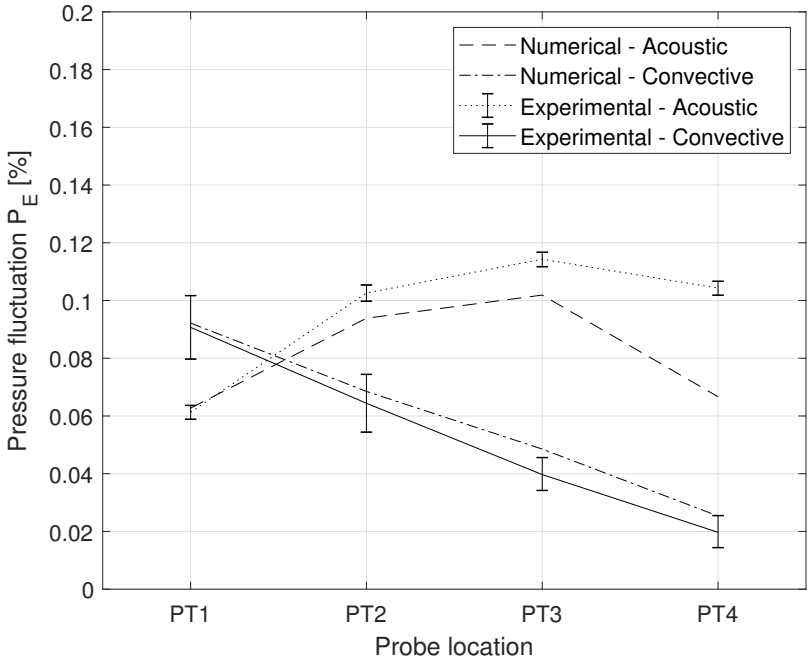

Figure 10. Numerical and experimental pressure decomposed into convective and acoustic components

expected, the second setup results in a stiffer turbine and higher eigenfrequency. Note however, that both harmonic simulations are performed at numerical resonance. The two simulations give different deformation patterns and also different pressure distribution in the runner channels. This leads our case to an increase in the pressure amplitudes in the probes. The two cases presented here are the extreme variations, it is likely that the true trailing edge connection is somewhere in between what is shown in figure 12.

By combining the effects seen in figure 11 and 12 it would be possible to be well within the experimental uncertainty in all pressure probes. This has not been done, but it illustrates the importance of investigating and documenting the sensitivity to the key parameters in the simulations, especially if no experimental results are available for validation.

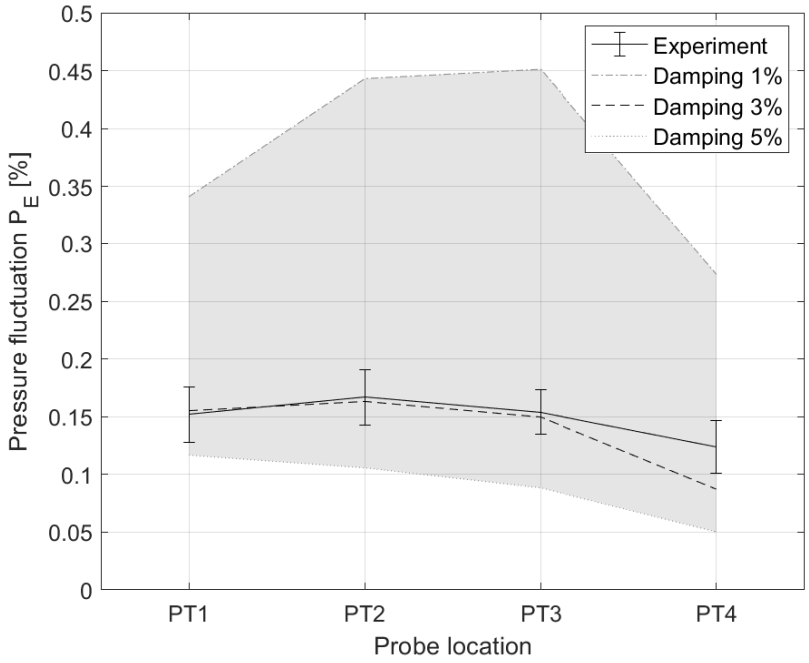

Figure 11. Sensitivity of pressure amplitudes to damping

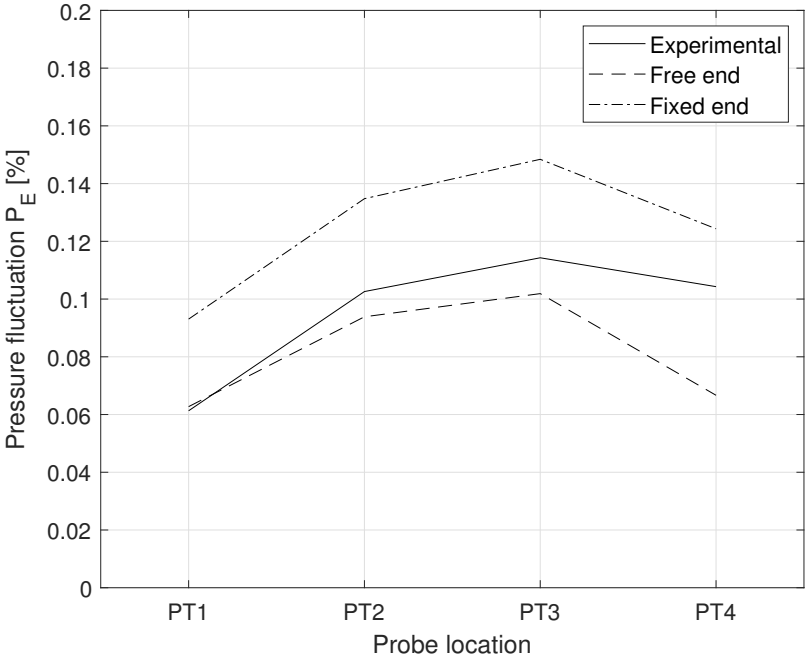

Figure 12. Acoustic pressure with different fixation of the blade to shroud close to the trailing edge

3.2. Two-way coupled simulation

Figure 13 shows the normalized structural deformation resulting from the RSI pressure field. Nodal diameter 2 is observed. A visual inspection of the time-series of the blade deformation, or a Fourier transform of the same signal, reveals that also the ND=4 is present. This is a nice validation of the Tanaka formula, eq. 3, which predicted ND2 and ND4 for the given combination of guide and runner vanes.

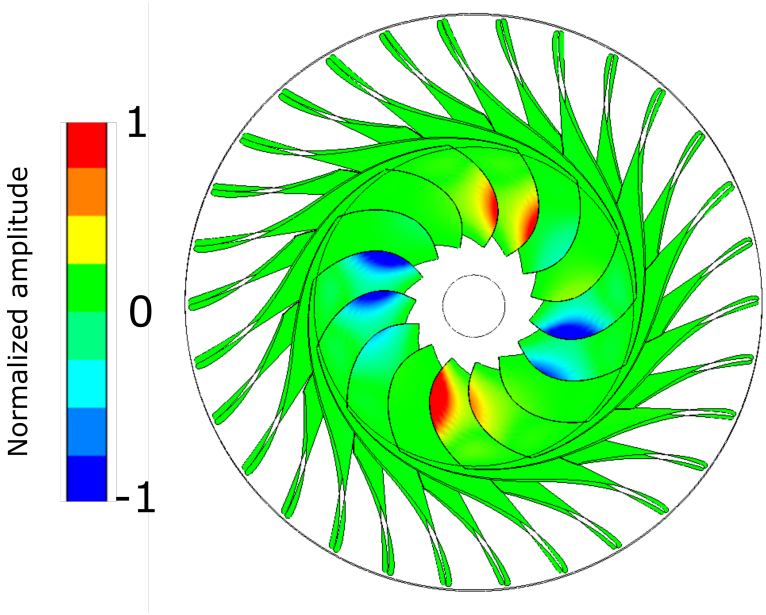

Figure 13. Normalized blade deflection from Two-way simulation, seen from the outlet.

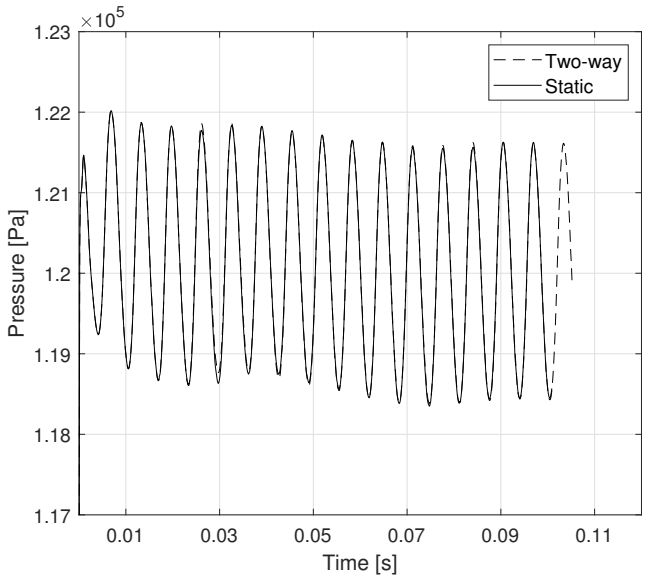

Figure 14. Pressure time series from CFD (static) and Two-way simulation

Figure 14 shows the pressure signal in one pressure probe for two simulations; one with stationary blades, in the other, the blades are allowed to deflect, as shown in figure 13. There is close to no difference in the pressure values.

Taking one step back, we can define the goal from the two-way simulations by the following questions;

- Does the pressure field from the RSI excite the expected Nodal Diameters?
- Does the vibration of the blades change the pressure pulsations in the channels compared to rigid blades?

Figure 13 clearly shows that the first is true. The second question is whether it is a coupling between the structural deflection and the pressure, i.e. if this procedure can be used to capture the resonance phenomena. Figure 14 shows that this is not the case. There is no difference in the pressure through the channel. The magnitude of the deflection is in the same order as the coupled acoustic-structural simulations in section 3.1, indicating that too small deflections is not the cause for the lack of pressure amplification.

The current setup for the FSI - MOR have some clear limitations. The lack of a complex description of the structural decomposition means that only real deformations can be simulated. This was partially circumvented in this paper, but introduces a general uncertainty. Also, the structural model with fixed trailing edge had to be used as the CFD mesh cannot handle relative motion between hub/shroud and blade at the joint. This meant that the imported structural eigenfrequency (or stiffness) was artificially high. Two options are available to mitigate this; firstly, the eigenfrequency can be modified, at the risk of losing the consistency between modal amplitude and stiffness. Another option is to change the rotational speed of the runner along with the head and flow to ensure hydraulically identical conditions. The question then is the predictive value of the simulation as the load frequency is knowingly to high.

The biggest limitation however, in the current setup, is believed to be the lack of compressibility. As was seen in figure 10, the contribution of the acoustic pressure is significant and necessary to predict the true pressure in the channel. Acoustic pressure is impossible to simulate in an incompressible simulation with no speed of sound. The medium (water) is unable to transmit pressure waves described by eqs. A.8.

4. Conclusions

Two different fluid-structural coupling procedures are presented in order to capture the resonance effect in a Francis turbine runner channel. The acoustic-structural coupling is successful in replicating the experimental results to a good degree. Complex bolting and connections in the Francis-99 model turbine creates uncertainties in the numerical simulations, in particular the fixation of the blade close to the trailing edge. Additionally, the amplitude at resonance is very dependent on the damping. If a damping estimate is not available from experiments, a flutter analysis should be performed to obtain a proper input.

The two-way simulation using a reduced order structural model did not produce the resonance phenomena. The reason for this is believed to be the lack of compressibility, which means that the acoustic pressure is not captured. This indicates that the use of the procedure should be limited to cases where the assumption of incompressibility is valid.

Acknowledgement

This work was done in the HiFrancis project, supported by the Norwegian Research Council and the Hydropower industry in Norway.

References

[1] Billah K Y and Scanlan R H 1991 *American Journal of Physics* **59** 118–124
[2] Østby P, Billdal J T, Sivertsen K, Haugen B and Dahlhaug O G 2016 *Int. J. Hydropower Dams* **23** 88–92
[3] Francis-99 research project `https://www.ntnu.edu/nvks/francis-99` accessed: 2019-03-12
[4] Trivedi C, Cervantes M and Dahlhaug O 2016 *Energies* **9** 74
[5] Agnalt E, Østby P, Solemslie B W and Dahlhaug O G 2018 *Shock and Vibration* **2018**
[6] Kundu P K, Cohen I M and Dowling D 2008 Fluid mechanics 4th
[7] Hifrancis research project `https://www.ntnu.edu/nvks/hifrancis` accessed: 2019-03-12
[8] Jakobsen K R G, Tengs E and Holst M A 2019 *IOP Conference Series: Earth and Environmental Science* **240** 072001
[9] Benra F K, Dohmen H J, Pei J, Schuster S and Wan B 2011 *Journal of applied mathematics* **2011**
[10] Ansys® mechanical apdl, release 19.3, theory reference, acoustics, ansys, inc.
[11] Everstine G 1997 *Computers & Structures* **65** 307–321
[12] Puri R S, Morrey D, Bell A J, Durodola J F, Rudnyi E B and Korvink J G 2009 *Applied Mathematical Modelling* **33** 4097–4119
[13] Tanaka H 2011 *International Journal of Fluid Machinery and Systems* **4** 289–306
[14] Franke G, Powell C, Fisher R, Seidel U and Koutnik J 2005 *Sound and Vibration* **39** 14–18
[15] Johnson metall - alloys `http://www.johnson-metall.com/en/product-data-sheets` accessed: 2019-03-12
[16] Celik I B, Ghia U, Roache P J *et al.* 2008 *Journal of fluids {Engineering-Transactions} of the {ASME}* **130**
[17] Craig R R and Kurdila A J 2006 *Fundamentals of structural dynamics* (John Wiley & Sons)
[18] Tengs E and Einzinger J 2019 Two-way coupled simulation of the francis-99 hydrofoil using model order reduction *Journal of Physics: Conference Series* (Accepted for publication)
[19] Jakobsen K R G and Holst M A 2017 Cfd simulations of transient load change on a high head francis turbine *Journal of Physics: Conference Series* vol 782 (IOP Publishing) p 012002
[20] Tengs E O, Bergan C W, Jakobsen K R and Storli P T 2019 *IOP Conference Series: Earth and Environmental Science* **240** 062002
[21] Zienkiewicz O C, Taylor R L and Zhu J Z 2005 *The finite element method: its basis and fundamentals* (Elsevier)

Appendix A. Derivation of the Eulerian displacement-pressure formulation

In the following section, the basic equations for solving acoustic problems will be presented. Most of the derivation can be found in [6], and ANSYS specific implementation can be found in [10]. Starting with the continuity equation;

$$\frac{d\rho}{dt} = -\nabla \cdot (\rho \overline{v}) + Q \tag{A.1}$$

Where ρ is the density, v is the velocity vector, and Q is a mass source. The Navier-Stokes equation can be written as follows;

$$\rho[\frac{d\overline{v}}{dt} + v \cdot \nabla v] = -\nabla p + \nabla \cdot \tau + \rho \overline{b} \tag{A.2}$$

Where τ is the shear tensor. For simplicity, we assume no body forces $\overline{b}$, no mass source Q, and no mean velocity from this point on. Also assume small pertubations such that a linearization is possible;

$$\begin{aligned} p &= p_0 + p' \\ \rho &= \rho_0 + \rho' \\ v_i &= 0 + v_i' \end{aligned} \tag{A.3}$$

Where the subscript 0 denotes constant values, and the prime denotes the fluctuating part, small relative to the respective constants. Inserting the above into the continuity and Navier-Stokes equation respectively;

$$\frac{d\rho'}{dt} = -\nabla \cdot (\rho v') \tag{A.4}$$

and,

$$\rho_0 \frac{dv'}{dt} = -\nabla p' + \nabla \cdot \tau \tag{A.5}$$

For newtonian fluids, the stress tensor can be written as a sum of a "shear" part and a compressibility part,

$$\tau = \mu(\nabla v + (\nabla v)^T) + \lambda(\nabla \cdot v)I \tag{A.6}$$

Where μ is the dynamic viscosity, and λ is the "second" or volume viscosity, given as $\lambda = -\frac{2}{3}\mu$ by the Stokes approximation [6]. The above is usually a very convenient split, as only the first term is applicable in incompressible simulations (where $\nabla \cdot v = 0$). Substituting the above into the Navier-Stokes, noting that the flow is irrotational, gives the following [10];

$$\rho_0 \frac{dv'}{dt} = -\nabla p' + \frac{4\mu}{3}\nabla(\nabla \cdot v') \tag{A.7}$$

To obtain the wave equation, subtract the space derivative of the Navier-Stokes equation from the time derivative of the continuity equation:

$$\nabla^2 p' - \frac{1}{c^2}\frac{d^2 p'}{dt^2} + \nabla \cdot [\frac{4\mu}{3}\nabla(\nabla \cdot v')] = 0 \tag{A.8}$$

Where we have used the isentropic definition of the speed of sound, c [6];

$$c^2 \simeq \frac{p'}{\rho'} \tag{A.9}$$

The known Galerkin method is used to formalize the finite element formulation. Eq. A.8 is mulitiplied by a testing function w, and integrated over the domain. This procedure is well explained in a number of FEA text books, i.e. [21], and ANSYS' own documentation [10], and yields the following after some manipulation;

$$\iiint_\Omega \frac{1}{\rho_0 c^2} w \frac{d^2 p'}{dt^2} dV + \iiint_\Omega \nabla w \cdot (\frac{4\mu}{3\rho^2 c^2} \nabla \frac{dp}{dt}) dV + \iiint_\Omega \nabla w \cdot (\frac{1}{\rho_0} \nabla p') dV + \oiint_\Gamma w \overline{n} \cdot \frac{d^2 v'}{dt^2} = 0 \tag{A.10}$$

The above representation is rewritten to matrix form using element shape functions;

$$\begin{aligned} p &= N^T p_e \\ u &= N'^T u_e \end{aligned} \tag{A.11}$$

where N, N' are the shape functions for the pressure and displacements respectively. p_e, u_e is the nodal pressure and displacements. Insert the shape function representation into equation A.10, and rewrite on matrix form;

$$M_a \ddot{p}_e + C_a \dot{p}_e + K_a p_e + \rho_0 R^T \ddot{u}_e = 0 \tag{A.12}$$

where the acoustic matrices are defined as follows [10];

$$\begin{aligned} M_a = \rho_0 \iint_\Omega \frac{1}{\rho_0 c^2} N N^T dV, \quad C_a = \rho_0 \iint_\Omega \frac{4\mu}{3\rho_0^2 c^2} \nabla N^T \nabla N dV \\ K_a = \rho_0 \iint_\Omega \frac{1}{\rho_0} \nabla N^T \nabla N dV, \quad R^T = \oiint_\Gamma N \overline{n} (N')^T ds \end{aligned} \tag{A.13}$$

Note that the acoustic wave equation written on a matrix form, eq. A.12 is similar to the known second order structural equation;

$$M\ddot{u} + C\dot{u} + Ku = F \tag{A.14}$$

The two equations, A.12 and A.14 can now be combined, rewritten on a harmonic form by assuming that all unknowns behave harmonically, to the Eulerian displacement-pressure formulation [10, 11, 12]:

$$\left(-\omega^2 \begin{bmatrix} M_s & 0 \\ M_{fs} & M_a \end{bmatrix} + i\omega \begin{bmatrix} C_s & 0 \\ 0 & C_a \end{bmatrix} + \begin{bmatrix} K_s & K_{fs} \\ 0 & K_a \end{bmatrix} \right) \begin{Bmatrix} u \\ p \end{Bmatrix} = \begin{Bmatrix} F_s \\ F_a \end{Bmatrix} \tag{A.15}$$

The matrices (M_{fs}, K_{fs}) can be shown to be $(\rho_0 R^T, -R)$ respectively [10].